Accepted for Publication in Water Resrources Research, 2003

Field-Scale Estimation of Volumetric Water Content using GPR Groundwave Techniques

K. Grote [1], S. Hubbard [1,2], Y. Rubin [1]

[1] Dept. of Civil and Env. Engineering, UC Berkeley, Berkeley, CA 94720 krgrote@lbl.gov

[2] Lawrence Berkeley National Laboratory, Berkeley, CA 94720

Abstract

Ground penetrating radar (GPR) groundwave techniques were applied to estimate soil water content in the uppermost ~10 cm of a 3 acre California vineyard several times over one year. We collected densely spaced GPR travel time measurements using 900 MHz and 450 MHz antennas and analyzed these data to estimate water content. The spatial distribution of water content across the vineyard did not change significantly with time, although the absolute water content values varied seasonally and with irrigation. The GPR estimates of water content were compared to gravimetric water content, time domain reflectometry (TDR), and soil texture measurements. The comparisons of GPR-derived estimates of water content to gravimetric water content measurements showed that the GPR estimates had a root mean square error of volumetric water content on the order of 0.01. The results from this study indicate that GPR groundwaves can be used to provide non-invasive, spatially dense estimates of shallow water content over large areas and in a rapid manner.

1. Introduction

Monitoring near-surface soil water content is a vital component for agricultural, ecological, meteorological, and vadose zone programs and for rational water resources management. The information obtained from monitoring water content at agricultural sites is critical for optimizing crop quality, achieving high irrigation efficiencies, and minimizing lost yield due to waterlogging and salinization. Water content monitoring is also important for addressing issues of water resources, needed for managing the environmental impacts of irrigated agriculture and for protecting functional ecosystems. Finally, near surface water content is an important parameter for understanding vadose zone processes such as evapotranspiration, partitioning of precipitation into surface runoff or groundwater storage, and as input into meteorological models.

For precision agriculture in vineyards, estimates of the shallow soil water content are used to improve fruit quality and irrigation efficiency. Information about soil water content ranges and spatial patterns can also be used prior to planting to optimize vineyard layout. Water content is often assessed for vineyard applications using conventional tools such as gravimetric sampling, time domain reflectometry (TDR), frequency domain reflectometry, neutron probe logging, tensiometers, and electrical resistance and thermal dissipation in porous blocks (Pritchard, 1999). These methods may provide reasonable water content estimates, but they are invasive and disturb the soil structure, and thus the obtained measurements may not represent in-situ moisture conditions. Additionally, near-surface water content is a function of properties such as topography, precipitation, evapotranspiration, geology, and vegetation (Western et al., 1998). These properties are spatially and sometimes temporally variable, so collection of enough measurements to adequately capture the spatial distribution of water content within a vineyard can be challenging using point measurements. An alternative to conventional methods

for estimating water content is satellite-based remote sensing, which uses infrared and microwave frequencies to estimate water content in the uppermost 0-5 cm of soil (Jackson et al., 1996). Remote sensing techniques permit estimation of water content quickly and over very large areas, but typically provide poor resolution; the highest resolution possible from spaceborne sensors is currently on the order of 100 m (Jackson et al., 1996; Mancini et al., 1999). Remote sensing measurements are affected by factors such as surface roughness, illumination geometry, and system parameters (Mauser et al., 1994), and must be calibrated before conversion into water content estimates. Finally, remote sensing techniques require an exposed soil surface to estimate the water content. Since the leaf canopy area is often quite large at agricultural sites, remote sensing techniques are often impractical for obtaining water content information to guide precision agriculture.

Our research focuses on investigating the applicability of a near-surface geophysical technique, ground penetrating radar (GPR), for estimating water content at spatial scales in between those of conventional point measurements and remote sensing data. In this paper, we concentrate on information obtained from GPR groundwaves, which travel in the shallow subsurface from a ground-based transmitter to a ground-based receiver. As the GPR groundwave measurement depth is partially a function of frequency, groundwave data can potentially be used to estimate the near-surface water content profile by analyzing data collected at different frequencies. GPR groundwaves may quickly provide water content estimates with a vertical resolution comparable to that of conventional methods such as TDR and gravimetric sampling, but in a non-invasive manner and with much greater lateral resolution. Thus, the GPR groundwave approach has the potential to provide much denser estimates of in-situ water content

over large areas, which could lead to an improved understanding of the three-dimensional variability of water content within an area.

The primary goals of this experiment were to develop data collection and interpretation techniques for obtaining reasonable and rapid estimates of near-surface water content using GPR groundwave travel time data, to validate GPR-obtained water content estimates through comparison with conventional point-based measurements, and to compare GPR estimates of water content with soil texture data. After development of the data acquisition and interpretation techniques, we applied GPR groundwave technology to a heterogeneous field site located near the Robert Mondavi Winery in Napa, California to estimate temporal and spatial variations in water content under natural field conditions. A brief background of water content estimation methods using GPR groundwaves is given in Section 2, and the site description and data collection procedures for this experiment are presented in Section 3. Section 4 describes the data interpretation and validation techniques and the correlations between the different types of measurements. The results of applying the data interpretation techniques to estimate water content across the entire field site at different times during the year are discussed in Section 5.

2. Background of GPR Groundwaves

GPR is a geophysical technique that uses high frequency (~50-1500 MHz) electromagnetic energy to probe the subsurface. Energy is emitted from the GPR transmitter as a spherical wave, and some of this energy travels along the air-ground interface in the near subsurface toward the receiver. This energy creates a boundary wave that is referred to as the groundwave. As described in detail by Berktold et al. (1998), the groundwave is confined to the air-ground boundary. It can be challenging to determine the exact depth of influence of the groundwave (z). However, many characteristics of radar data are similar to those of seismic

data, and the approximate depth of influence for seismic groundwaves is determined as half of the Fresnel zone (Hagedoorn, 1954). Van Overmeeren et al. (1997) adapted the seismic approximation for use with GPR groundwaves, and expressed the depth of influence as:

$$z = \frac{1}{2}\sqrt{\frac{vS}{f}} \ , \tag{1}$$

where v is the electromagnetic velocity of the near-surface material, S is the separation distance between the transmitting and receiving antennas, and f is the central frequency of the GPR signal. This expression indicates that the depth of influence of the groundwave is greater in dry soils, which have higher velocities, than in wet soils. Also, the expression suggests that signals having lower central frequencies will have a deeper zone of influence than signals having higher central frequencies.

The electromagnetic velocity of the near-surface soils can be calculated from the groundwave using variable-offset or common-offset GPR acquisition geometries. Variable-offset surveys are collected by moving the transmitter and receiver apart by constant increments for each measurement. One commonly used form of variable-offset surveying is the common-midpoint (CMP) survey, where both the transmitter and receiver are displaced for each measurement. As the distance between the antennas increases with each measurement in a variable-offset survey, the time that it takes for the groundwave to travel between antennas, or the travel time, also increases. The electromagnetic velocity of the soil is calculated as the inverse of the linear slope created by the groundwave travel time and antenna separation measurements.

Common-offset surveys are collected when the transmitting and receiving antennas are kept at a constant separation distance and are moved in parallel along a traverse. For common-

offset surveys, the travel time of the groundwave is determined relative to the arrival time of the airwave. The airwave is energy that also travels directly from the transmitter to the receiver, but it travels through the air at the speed of electromagnetic waves in a vacuum (c). The airwave velocity ($3x10^8$ m/s) is faster than the groundwave, so the airwave arrives earlier in time and can be used as a reference for calculating the 'zero time'. Subtraction of this zero time from the arrival time of the groundwave yields the time needed for the groundwave to travel from the transmitter to the receiver. The groundwave velocity can then be determined from common-offset data by dividing the distance between the transmitting and receiving antennas by the travel time of the groundwave across this distance. Once the groundwave velocity has been calculated using either the variable-offset or common-offset surveying method, it can be used to estimate the dielectric constant (κ) using an approximation appropriate for high radar frequencies in soils having low electrical conductivities (Davis and Annan, 1989):

$$\kappa \approx \left(\frac{c}{v}\right)^2 . \qquad (2)$$

The electromagnetic velocity can be frequency dependent, in which case the approximation given in (2) cannot be applied. This is especially true for low radar frequencies and within fine-grained, chemically reactive soils such as clays, where the polarization of bound water at the soil-water interface is frequency dependent. However, researchers have found that the frequency dependence of clay soils is significant only at frequencies less than 300 MHz (Olhoeft and Capron, 1994), while other studies show that the frequency dependence of interfacial polarization does not contribute appreciably to the dielectric response for frequencies greater than 50 MHz (White and Zegelin, 1995). Thus, for the higher frequency data (450 MHz and 900 MHZ) acquired in this experiment, variations in dielectric constant between the two frequencies

are most probably caused by different sampling depths rather than by frequency dependence of the fine-grained component of the vineyard soil.

For high frequency GPR data, such as used in this study, the dielectric constant of unsaturated soils is primarily dependent upon the water content of the soil, though other factors such as lithology, temperature, particle shape, and pore fluid composition may also contribute to the GPR response. Water content greatly influences the dielectric constant of soil because there is a large contrast in dielectric constant values between dry geologic materials (~3-8), water (~81), and air (~1). Thus, variations in the amount of water in the soil pores greatly change the dielectric constant of the soil. Petrophysical models can be used to relate the dielectric constant to water content; these models can be developed for a specific soil or can be borrowed from literature.

Several researchers have used GPR groundwave travel time data to estimate water content in the shallow subsurface. Du and Rummel (1994), van Overmeeren et al. (1997), and Huisman et al. (2001) used variable-offset data to estimate water content from the groundwave velocity. While variable-offset data can provide accurate estimates of water content, this surveying mode is too time-consuming and labor-intensive for collection of the many measurements that are needed to adequately estimate the variations in water content over space and time at the field scale. Additionally, variable-offset data have large sample volumes and thus lower spatial resolution than typical common-offset GPR data. As an alternative to conventional variable-offset GPR surveys, GPR systems with multiple receiving antennas may allow data to be collected at several different offsets with data acquisition speeds similar to those of common-offset surveys. However, these systems are not yet commercially available, and processing data acquired with multiple receivers can be time-consuming and thus may prohibit

rapid data analysis. Du and Rummel (1994) overcame the limitations associated with variable-offset data acquisition and processing by estimating the water content from common-offset groundwave data, after using variable-offset surveys to identify the groundwave and airwave arrivals on the common-offset data. Although they did not verify their volumetric water content estimates along the common-offset traverse, they observed that the common-offset GPR measurements showed lower water content values in coarse-grained soils than in clayey soils. Lesmes et al. (1999) followed this approach to estimate water content in a 17 m^2 area using a grid of low-frequency (100 MHz) common-offset GPR groundwave data. They compared the resulting GPR estimates of water content to measurements of water content obtained using TDR and gravimetric sampling. Their GPR estimates followed the same trends as the conventional measurements, but the absolute values of water content were significantly less than those found with conventional methods, possibly due to different sampling depths for low frequency GPR and conventional techniques. However, Huisman et al. (2001) collected co-located higher frequency (225 MHz and 450 MHz) variable-offset groundwave data, TDR, and gravimetric measurements at several small (5 m x 2 m) study plots and found that the groundwave velocities produced estimates of water content that agreed well with both the TDR and gravimetric water content measurements.

The previous studies have shown that GPR groundwaves can be used both qualitatively and quantitatively for water content estimation. This experiment expands upon these previous encouraging studies by testing the utility of GPR as a field tool for rapidly and accurately providing high-resolution estimates of volumetric water content under naturally heterogeneous conditions. Specifically, we investigate the use of high-frequency (450 MHz and 900 MHz) common-offset GPR groundwaves for obtaining densely spaced estimates of water content over

a large-scale agricultural field as a function of space and time. In addition to investigating spatial and temporal variations in water content and their relationship to precipitation and irrigation, we also compare our volumetric water content estimates with gravimetric water content, TDR, and soil texture measurements.

3. Site Description and Data Acquisition

3.1. Site description

The study site is located next to the Robert Mondavi Winery near the town of Oakville in Napa County, California. The study site is approximately 12,000 m^2 and is planted with grapevines having row and vine spacing of 1.2 m each. The soils in the study area are generally described as belonging to the Bale series of the USDA Soil Conservation Service Classification System, which are somewhat poorly drained soils deposited in alluvial fan, flood plain, and low terrace settings and are derived from rhyolite and basic igneous rocks (Lambert et al., 1978). The texture of the soil varies from sandy loam to clay loam, with the most common textures being sandy loam and sandy clay loam. Topographic variations across the study site are negligible, and the water table is approximately 4 m below ground surface. Summers are hot and dry; most precipitation occurs during the cool winters. The mean annual precipitation for this area is 0.64 to 0.89 m. The site is watered uniformly using a drip irrigation system during the driest months, approximately from June to October, with an average irrigation rate of 0.002 m/day.

Remote sensing data were used as a factor in choosing the study site. Remote sensing data were acquired at the Mondavi site in August 1998, August 1999, and July 2000 using airborne ADAR Multispectral System 5500 (Positive Systems) collecting in the blue, green, red and near-infrared portions of the spectrum from a flight altitude of 4300 m above the ground

surface and with a spatial resolution of 2m x 2m (Johnson et al., 2000). These data were processed to yield normalized difference vegetation index (NDVI) data, which relate the proportions of photosynthetically absorbed radiation in the visible and near-infrared wavelengths. NDVI data can be correlated to the density, or vigor, of vegetation. Variations in NDVI within an area often reflect differences in irrigation, nutrient availability, vineyard geometry, rootstock, and disease or pest infestation (Penn, 1999; Carothers, 2000). The site map shown in Figure 1 is superimposed on NDVI imagery collected in July 2000; in this image the darker areas indicate weak vegetation, and the lighter zones signify more vigorous vegetation. The NDVI images from the three data sets collected at this site are all very similar, suggesting that the same factors influence vegetation vigor each year. At this site, all agricultural parameters (vine and row spacing, trellis type, and rootstock) and management practices (irrigation, fertilization, and pruning) are constant throughout the vineyard. The uniformity of these parameters suggests that the variations in vegetation vigor shown by the NDVI data may be a function of soil texture and moisture availability. The variability displayed in the NDVI data was one of the factors used in selection of the field site, as one of our goals was to investigate the influence of spatially variable soil texture on soil water content.

3.2. Data acquisition

We collected several different types of data at the study site, including surface GPR, gravimetric water content, TDR, and soil texture data. Figure 1 shows the site geometry and the location of many of these measurements. Surface GPR data were collected using a Sensors and Software PulseEkko1000 system at central frequencies of 450 MHz and 900 MHz, with bandwidths approximately equal to the central frequency. We collected very high-resolution common-offset and variable-offset GPR data over selected 1-m Dense Sampling Areas (DSAs)

throughout the field in September 2001, November 2001, and January 2002 as shown on Figure 1. Data collected at the DSAs were used to develop groundwave interpretation techniques and to compare the accuracy of the water content estimates obtained from GPR data with co-located point measurements obtained from conventional methods, as will be discussed in Section 4. Data grids were also collected across the entire field using the common-offset GPR acquisition mode. Each grid contained traverses collected at least every fifth row between rows 35 and 155 (Figure 1), and data were acquired along each traverse with a spatial sampling (trace) increment of 10 cm. Data grids were collected over the entire field site over a nine-month period during four field campaigns; the campaigns occurred in May 2001, August 2001, September 2001, and January 2002. The data campaigns were scheduled to capture the major seasonal variations in water content at the site. The May campaign occurred after the rainy season but before irrigation, the August and September data were collected in the hot, dry summer during irrigation, and the January campaign was performed in the wet winter. Weather conditions were sunny for all of the data campaigns. Interpretation of the data grids following the procedure developed in the DSAs will be discussed in Section 5.

Except for the spatial sampling increment, the same GPR acquisition parameters were used when collecting data over the entire field or within the DSAs. The antenna separation for common-offset surveys was 17 cm for the 900 MHz antennas and 25 cm for the 450 MHz antennas. Common-offset data for both frequencies were collected at 2-cm spatial sampling increments in the DSAs and 10-cm sampling increments for the grids for all campaigns. CMP surveys for both frequencies were collected in the DSAs starting with an antenna separation of 17 cm and increasing the separation by increments of 2 cm or 2.5 cm to a final antenna separation of at least 1 m. For all campaigns, the time sampling increment was 100 picoseconds

for the 900 MHz data and 200 picoseconds for the 450 MHz data. The data were stacked 16 to 32 times at each acquisition station to enhance the recorded GPR signal over random noise contributions. Data processing was minimal. Bandpass filtering was performed on the common-offset and CMP data to remove very low frequency components and high frequency noise. Automatic gain control was applied to the CMP data to increase the amplitudes at longer antenna separations, but no amplitude balancing was applied to the common-offset data. For data collected during very dry times, FK filtering (Yilmaz, 1999) was applied to the CMP data to remove airwave 'ringing' and thus to minimize airwave and groundwave interference, which produced more accurate groundwave velocity estimates.

Gravimetric water content, soil texture, and TDR measurements were also collected within the DSAs. Gravimetric water content and soil texture (percent sand, silt, and clay of the non-gravel component) were determined from near-surface soil samples, using ASTM standard procedures D2216 for the water content measurements and C136 and D422 for the soil texture measurements. The average sample volume for both the gravimetric water content and textural analyses was 250 cm^3. For the samples collected in the DSAs, two samples were usually taken over the interval from 0-10 cm depth and two samples taken over 10-20 cm depth. One sample from each depth interval was analyzed for water content, and the other was analyzed for soil texture. Soil texture measurements were also taken from the first sample collected in each of the boreholes shown in Figure 1 and were analyzed using the same methods as the near-surface samples. These borehole samples were collected over 0-30 cm depth. TDR data were collected using a SoilMoisture Trase System with two 15-cm waveguides placed 5 cm apart and a central frequency of approximately 3 GHz. The average sample volume of a TDR measurement is a cylinder of approximately 750 cm^3 centered around the waveguides. The near-surface

gravimetric water content, soil texture, and TDR measurements were taken coincidently with the GPR data within the DSAs. These point measurements were taken at the center of each 1-m traverse for calibration and validation of the GPR data.

4. Development of Interpretation Procedure and Petrophysical Relationships using Detailed Study Areas (DSAs)

In this section, we discuss the development and validation of the methodology used to estimate volumetric water content from GPR groundwave data collected in the DSAs. The first part of this discussion describes the techniques used to estimate groundwave velocities using CMP and common-offset GPR data. Next, we develop a site-specific petrophysical relationship using TDR, gravimetric water content, and soil texture measurements. Finally, the petrophysical relationship is applied to the GPR velocity estimates, and the resulting water contents are compared to the gravimetric water content measurements. In addition to the GPR-derived water content estimates, we also discuss the correlations between dielectric constants from TDR and GPR and between water content and soil texture within the DSAs.

4.1. Estimation of groundwave velocity

Before the groundwave velocity can be estimated from common-offset GPR data, the airwave and groundwave signals must be correctly identified, and the travel time difference between the airwave and groundwave (Δt) must be calculated. A straightforward technique for identifying airwave and groundwave signals in common-offset GPR data is given in Du and Rummel (1994), who collected variable-offset data by increasing the separation distance of the antennas until the airwave and groundwave were easily identifiable. They then collected common-offset data at the antenna separation that was identified as optimal. This technique permits a clear identification of the airwave and groundwave and is the preferred method for

interpreting groundwave data. Because we decided to use commercially available antenna frames, our choices of common-offset antenna separation distances were limited. The PulseEkko1000 GPR equipment that we employed has three commercially available transmitter-receiver frames, which allow the antennas to be separated by 17 cm, 25 cm, or 50 cm when collecting common-offset data. Although frames can be manufactured by individuals to optimize the transmitter-receiver separation distance for specific water content conditions, we chose not to do this because of the possible errors that can be introduced by adding or modifying equipment (Huisman and Bouten, 2002).

We collected CMP surveys in soils with different textures and at different water contents. Based on analysis of these data, we determined which of the available antenna frames would be optimal on average for collecting common-offset 900 MHz and 450 MHz data grids under varied conditions. From the CMP data, we found that interference between the airwave and groundwave sometimes occurred under dry conditions at the smallest offsets. However, at far offsets and under dry conditions, the groundwave was more attenuated and was sometimes obscured by airwave ringing. We found that we could reasonably compensate for the effects of interference by picking portions of the airwave and groundwave wavelets that did not suffer interference at small offsets (as will be discussed below), but it was more challenging to compensate for interference due to airwave ringing or low signal quality at the further offsets. Through analysis of CMP and common-offset data in the DSAs, we determined that the highest quality signals at our site usually occurred at an antenna separation of 17 cm for the 900 MHz antennas and 25 cm for the 450 MHz antennas, and we used those antenna separations for all of our subsequent common-offset acquisition campaigns.

An example of a 900 MHz CMP survey collected at a DSA in January is shown in Figure 2a. The horizontal axis shows the antenna separation for each measurement, while the vertical axis is the travel time of the electromagnetic energy. On our wiggle-trace data, positive amplitudes are shown as peaks (black) while negative amplitudes are shown as troughs (white). Approximate airwave and groundwave 'picks' (where the arrival times are chosen) are indicated, as are the velocities for these waves. By comparison of common-offset and CMP data and following Annan (2002), the airwave was chosen as the first large-amplitude trough having the correct airwave velocity, and the groundwave was chosen as the first large-amplitude peak with a reasonable groundwave velocity. Choosing the first large-amplitude trough or peak for each wavelet reduces the effects of wavelet dispersion, although dispersion is not usually significant for radar data in non-magnetic soils for the frequencies used in this experiment (Olhoeft and Capron, 1994). The arrivals of the airwave and groundwave are generally very apparent on CMP gathers, as shown in Figure 2a. An example of common-offset data with airwave and groundwave picks is given in Figure 2b. This figure shows an interpreted 20-m segment of a 900 MHz common-offset survey line, collected in January at an antenna separation of 17 cm. These data are from one of the field grid lines (Row 115, vines 48-65) and are centered on the CMP survey shown in Figure 2a. In Figure 2b, each trace records the airwave and groundwave arrivals at a single surface location. The axes are similar to those in Figure 2a, but in Figure 2b the horizontal axis shows the location of the center of the transmitter-receiver pair for each measurement along the traverse. The picks for the airwave and groundwave in Figure 2b are based upon the arrival times and amplitudes of these events at a 17 cm offset in the CMP, and a commercially available processing package was used to automatically 'snap' the picks to the exact peak or trough of each trace given an approximate manual pick. Similarly, Figure 3a

shows a CMP of 450 MHz data collected in January in row 35. Figure 3b shows the corresponding 450 MHz common-offset data with an antenna separation of 25 cm along a 20 m traverse (row 35, vines 41-58) centered around the CMP shown in Figure 3a. The picks in the common-offset data correspond to the airwave and groundwave identified at 25 cm offset in the CMP data.

Picking the airwave and groundwave arrival times accurately was more complicated when the soil was very dry. At shorter antenna offsets and in dry soils, interference sometimes occurred between the airwave and groundwave. Superposition of portions of the airwave and groundwave usually caused the main airwave trough to appear to arrive later than it would without interference and caused the main groundwave peak to appear to arrive earlier. A modified picking procedure was developed to compensate for possible airwave and groundwave superposition at small antenna separations in the driest soils. The modified picking procedure utilized portions of the airwave and groundwave wavelets that did not appear to be superimposed. For example, minimization of the effects of superposition can be obtained by choosing an alternate airwave picking location with respect to the central airwave wavelet that arrives earlier in time than the main airwave trough, and if necessary, choosing an alternate groundwave picking location with respect to the central groundwave wavelet that arrives later in time than the main groundwave peak. A correction factor must then be applied to compensate for the time difference between the travel time calculated using the chosen picks and the travel time calculated using the 'true' airwave or groundwave. CMP data are most useful for identifying the modified picking location and calculating the correction factor, although common-offset data may also be used when adjacent soils of very different water contents adequately illustrate the effects of superposition.

An illustration of airwave and groundwave superposition and a modified picking procedure is given in Figure 4. This figure shows 900 MHz common-offset data collected using a 17 cm antenna separation in conjunction with an infiltration experiment that was performed prior to the full-field studies. In this experiment, approximately 4 gallons of water were applied along the indicated 1 m length in Row 145 in very dry soil, and a 4 m GPR traverse centered over the infiltrated area was subsequently collected, as shown in Figure 4. Following our picking procedure, we would typically choose the first large trough as the airwave arrival and the second large peak as the groundwave arrival; these arrivals are indicated by the heavy grey lines in Figure 4. However, it is clear that in the dryer zones outside of the infiltration zone, the airwave trough appears to be 'pulled down' in time relative to the wetter zone where no interference occurs. Additionally, the groundwave peak in the dry zones superimposes with an airwave peak, which could render exact picking of the groundwave peak difficult. To facilitate accurate airwave and groundwave picking under conditions of superposition, portions of the airwave and groundwave that do not appear to experience interference can be picked. For example, the airwave pick could be chosen as the small amplitude peak preceding the main airwave trough, and the groundwave pick could be chosen as the trough following the main groundwave peak. The correction factors for the modified picks of the airwave and groundwave are identifiable on this variably saturated common-offset GPR traverse and are shown in Figure 4. These correction factors must be subtracted from the difference in arrival times between the groundwave and airwave to compensate for the modified picking procedure. The travel time difference (Δt) is given as:

$$\Delta t = \Delta t_{modified} - \Delta t_{air,corr} - \Delta t_{ground,corr} \tag{3}$$

where $\Delta t_{modified}$ is the travel time difference using the modified airwave and groundwave picks and $\Delta t_{air,\ corr}$ and $\Delta t_{ground,\ corr}$ are the correction factors for the airwave and groundwave, respectively.

Once the arrival times were chosen for the airwave and groundwave, the difference in arrival times (Δt in Figures 2b and 3b) was calculated at each point along the common-offset traverses. However, this calculated difference is not the entire travel time of the groundwave between antennas, because the airwave (from which the 'zero time' is determined) also takes time to travel between the antennas. Some time must therefore be added to account for the travel time of the airwave before it is detected by the receiver. The travel time of the airwave from the transmitter to the receiver is calculated as the antenna separation (S) divided by the velocity of electromagnetic waves in air (c). This 'zero time adjustment' is added to each measured difference between the airwave and groundwave arrival times following Huisman et al. (2001). The final groundwave travel time (t_T) is given by:

$$t_T = \Delta t + \frac{S}{c}. \tag{4}$$

After the adjusted groundwave travel time was calculated for each location, the velocity was estimated using the common-offset antenna separation. The groundwave velocity was then converted to dielectric constant using eqn. (2).

To test the validity of our picking procedure for estimating the electromagnetic velocity from common-offset data under dry, average, and wet soil conditions, we compared the velocities estimated from CMP and common-offset data for each DSA. A plot of these velocities is shown in Figure 5. The strong correlation between velocities from CMP and co-located common-offset data indicates that the common-offset data produced accurate velocity

measurements. Differences in the velocities from the two methods may occur because the CMP velocity is more influenced by the center portion of the CMP survey than by the traces at longer antenna separations, while the common-offset velocity is an unweighted average of all the measurements along the traverse.

4.2. Development of a site-specific petrophysical relationship

The electromagnetic velocities, obtained as described in Section 4.1, were converted to dielectric constant estimates using eqn. (2). To estimate volumetric water content from these dielectric constants, a petrophysical relationship is needed. We developed a site-specific petrophysical relationship using co-located near-surface measurements of dielectric constant from TDR, gravimetric water content, and soil texture collected within the DSAs. The TDR measurements provided dielectric constant estimates at approximately the sampling depth expected for the GPR groundwaves, as will be discussed in Section 4.4. The gravimetric water content and soil texture measurements were used to estimate volumetric water content. Volumetric water content is calculated by multiplying the gravimetric water content by the bulk density of dry soil, then dividing this quantity by the density of water. In practice, measurement of the true soil bulk density is challenging, since undisturbed samples of non-consolidated soils are extremely difficult to collect, and valid density measurements cannot be taken from disturbed soil samples. To obtain reasonable estimates of the soil bulk density, we used the empirical method developed by Saxton et al. (1986) to estimate the soil density based upon the percentage of sand, silt, and clay in each sample. Using the estimated soil bulk density and an assumed a density for water of 1 g/cm^3, we converted the gravimetric water content measurements to volumetric water content estimates. We then developed a calibration equation following the semi-theoretical approach of Herkelrath et al. (1991):

$$\theta_v = a_1 + a_2\sqrt{\kappa}\,. \tag{4}$$

where a_1 and a_2 are empirically fitted calibration parameters. The data used to develop the petrophysical relationship and the resulting calibration equation are shown in Figure 6.

Before applying the TDR-based site-specific petrophysical relationship to GPR groundwave data, the differences in the sample volumes and frequencies of the TDR and GPR must be considered. Huisman et al. (2001) addressed these issues and showed that large-scale (up to 5 m antenna separation) GPR groundwave measurements and co-located gravimetric water content measurements produced empirical petrophysical relationships very similar to those obtained with small-scale TDR and gravimetric water content measurements for a variety of soils. From these results, Huisman et al. (2001) concluded that relationships developed using TDR are applicable to GPR groundwave data. White and Zegelin (1995) showed that dielectric constant (used to estimate water content) was independent of frequency in the ranges used by the GPR and TDR in this study. Also, other researchers (Du and Rummel, 1994; Greaves et al., 1996; Hubbard et al., 1997; Grote et al., 2002) have successfully applied TDR-based relationships to GPR data. Based upon these findings and the similar sample volumes measured by the TDR and GPR groundwaves, we determined that the TDR-based relationship developed at this site was applicable to GPR groundwave measurements of dielectric constant.

4.3. Validation of the water content estimation procedure using GPR groundwaves

We tested the accuracy of the data interpretation procedure (Section 4.1) and the site-specific petrophysical relationship (Section 4.2) on GPR data collected within the 1-m DSAs. Estimates of volumetric water content obtained from GPR groundwaves were compared to co-located estimates of volumetric water content obtained from gravimetric water content and soil

texture measurements collected from 0-20 cm depth in the middle of each GPR traverse, as described in Section 3.

Figure 7 shows the validation of our arrival time picking procedure and the site-specific petrophysical relationship on both CMP and common-offset data collected within the DSAs. As shown in Figure 7a, comparison of the volumetric water content estimates derived from CMP data and from gravimetric measurements showed a strong linear correlation for the 900 MHz data and a somewhat weaker correlation for the 450 MHz data. Estimates of water content from both frequencies had low root mean square errors (RMSE) of 0.015 and 0.022 for the 900 MHz and 450 MHz, respectively. Although these results suggest that CMP data can be used successfully for water content estimation, CMP surveys are time consuming to collect and interpret and so are not practical for field monitoring.

Common offset data, which can be collected and interpreted quickly, are preferable to CMP surveys for monitoring water content at the large field scale. Figure 7b shows the validation of our procedure using common-offset data. These data were acquired at 2 cm increments in each DSA, and the t_T values for each trace (following eqn. (4)) were averaged over the 1 m traverse to provide a single travel time measurement from common-offset GPR data for each DSA. This averaging also helped to reduce error due to imprecise location coordinates and to compensate for measurement error in individual GPR traces. The average travel time measurements were converted to water content estimates as described in Sections 4.1 and 4.2 and were compared to the volumetric water content values obtained from gravimetric sampling, as shown in Figure 7b. Both the 900 MHz and 450 MHz common-offset estimates correlated well with the water content from gravimetric sampling, with linear correlation coefficients (R) of 0.98 and 0.92, respectively. Also, the RMSE is small for both frequencies; the RMSE error is 0.011

for the 900 MHz data and 0.017 for the 450 MHz data. The higher error in the 450 MHz data may be caused by the lower resolution associated with the coarser time sampling increment and the longer wavelength of the 450 MHz data. For both frequencies, the RMSE of the common-offset data is less than that of the CMP data. The higher RMSE of the CMP data may be due to small errors in the position of the antennas during the variable-offset surveys, resulting in less accurate velocity estimates.

As shown by Figures 7a and 7b, the volumetric water content estimates obtained from CMP and common-offset data are somewhat different from those obtained gravimetrically. The estimates of volumetric water content from both the common-offset and CMP data show the greatest differences when compared to gravimetrically obtained water contents in the driest soils. For these soils, the GPR water content estimates are usually higher than the gravimetrically obtained measurements. A possible explanation for this bias is that the site-specific petrophysical relationship overestimates the water content in dry soils. During dry times, the vineyard soil is very hard, and the TDR probes must be carefully hammered into the ground to collect measurements. This forceful insertion of the TDR probes may create an air gap around the probes, which could cause the measured dielectric constant to be less than the true dielectric constant of the soil (Sakaki et al., 1998). If the TDR measurements (used to create the site-specific petrophysical relationship) underestimated the true dielectric constant, when the petrophysical relationship is applied to accurately measured dielectric constants, the water content will be overestimated. To determine if a more general petrophysical relationship would produce more accurate results, we applied the commonly used empirical Topp's equation (Topp et al., 1980) to the GPR data. Water content estimates from Topp's equation consistently overestimated the water content in both wet and dry soils, with greater overestimation occurring

in the wet soils. These estimates also had a much higher RMSE than that from the site-specific relationship. These results indicate that the site-specific relationship, although possibly inaccurate at low water contents, is nonetheless preferable for this site.

In addition to a possible bias in the petrophysical relationship under dry conditions, there are several other potential reasons for the differences between GPR estimates and gravimetric measurements of water content. One reason could be the different sampling volumes of the GPR signals and the gravimetric measurements. Another possible reason could be inaccuracies in the density estimates used to convert gravimetric water content measurements to volumetric water content estimates. Inaccuracies in the density estimates could create errors in the petrophysical relationship applied to the GPR data and in the volumetric water content values obtained from gravimetric measurements that are compared to the GPR-derived estimates. A third source of error may be airwave and groundwave interference, which could cause inaccuracies under dry conditions. Despite the possible reasons for error, the RMSE of both the 900 MHz and 450 MHz data are very small, and the accuracy of these estimates is quite sufficient for typical field applications such as precision agriculture.

4.4. Depth of influence of the GPR groundwaves

The common-offset travel time data collected within the DSAs were also useful for investigating the possible depth of influence of the groundwaves. To estimate the depth of influence using eqn. (1), we used the central frequencies observed in the data spectra, the average groundwave velocity from CMPs, and the measured antenna separation. These calculations show that for an antenna separation of 17 cm, the zone of influence for the 900 MHz data extends from the surface to approximately 7 cm in wetter soils and 10 cm in dryer soils. For the 450 MHz data with an antenna separation of 25 cm, the zone of influence is approximately

11 cm in wetter soils and 14 cm in dryer soils. These theoretical zones of influence were compared to near-surface gravimetric measurements sampled over two separate depth zones of 0-10 cm and 10-20 cm, as well as the average of the measurements in the two zones over the depth interval from 0-20 cm. Both the 900 MHz and the 450 MHz data show the highest correlation with the gravimetric water content averaged over 0-20 cm and the least correlation with the water content in the 10-20 cm interval. These correlations imply that the depth of influence for this data set may be slightly deeper than that predicted using eqn. (1), but that the predictions are reasonable. Differences in the water content estimates from the 900 MHz and 450 MHz data may also be indicative of the depth of influence for each frequency. The DSA campaign in November was performed one day after a light rainfall. The gravimetric water content samples showed that the soil in the 0-10 cm zone was wetter than the soil in the 10-20 cm zone. The common-offset GPR data collected on this date showed that the 900 MHz data produced higher estimates of water content than the corresponding 450 MHz estimates. Although these studies indicate that the 450 MHz data may have a deeper zone of influence than the 900 MHz data, gravimetric measurements taken at smaller vertical intervals during times of known vertical heterogeneity are necessary to accurately establish the depth of influence of each frequency.

4.5. Correlation of dielectric constant estimates from GPR groundwaves and TDR

TDR measurements were collected at the center of each 1-m DSA. Comparisons were made between dielectric constant estimates obtained from TDR data and from coincident GPR common-offset data averaged over the 1-m traverse. A plot of these data is shown in Figure 8. These data show that GPR and TDR produced similar dielectric constant estimates, despite the differences in measurement technique and sample volume. The slopes between TDR and GPR

estimates of dielectric constant are slightly greater than unity for both frequencies and are similar to the bias shown by the GPR data when compared to gravimetrically obtained volumetric water content estimates. This similarity implies that the apparent bias in the GPR water content estimates could be due to the TDR-based petrophysical relationship. The dielectric constant estimates from TDR and GPR are most different at low water contents, where the GPR dielectric constants are greater than the corresponding TDR estimates. Although it is not certain whether GPR or TDR is more reliable at low water contents for the conditions at the Mondavi site, the lack of correlation between these techniques at low water contents suggests that TDR-based petrophysical relationships should be developed with caution and that water content estimates in dry soils should be given wide error margins.

4.6. Correlation of water content and soil texture

Soil texture, as quantified by percent sand, silt, and clay, was measured coincidently with gravimetric water content during data collection at the DSAs, as described in Section 3. Figure 9 shows the correlations between percent sand and gravimetrically derived volumetric water content for each of the DSA data acquisition campaigns. This plot shows a correlation of decreasing water content with increasing percent sand for each data campaign. This result is expected for the near surface soils, as the soils with lower sand content (and thus higher fractions of silt and clay) will drain less easily and have higher average water contents.

5. Estimation of Spatial and Temporal Variations in Water Content Using GPR Grid Data

The interpretation techniques developed in the detailed study areas (DSAs) discussed in Section 4 were applied to the full-field grids of GPR data to assess near-surface variations in volumetric water content over space and time for the entire study site. Full-field GPR data were

collected at 900 MHz and 450 MHz along every fifth row as described in Section 3. The travel time data were analyzed and converted to water content as described in Section 4. The following discussion focuses on the full-field water content distributions with time, space, and depth as determined from the GPR travel time data and the comparison of the water content distributions with full-field soil texture data.

5.1. Estimation of water content using GPR travel time data

The water contents calculated from 900 MHz common-offset groundwave data for each full-field data campaign are shown in Figure 10. The average water content ($\overline{\theta_v}$) calculated from GPR estimates for each campaign is also given in this figure, and varies from 0.087 under the driest conditions to 0.247 under the wettest conditions. To reduce scatter in the full-field water content plots, a running average was computed for the GPR data, where an average value was calculated at the location of each of the GPR data points using the values of that point and the immediately adjacent points. The contour plots in Figure 10 show the water content distributions of the averaged values. Scatter was greatest between traverses (perpendicular to the vineyard rows), as the sampling interval in this direction was 6 m, in contrast to the sampling interval of 0.1 m along the rows. Figure 10 shows that the spatial distribution of water content is similar for all surveys, although the average water content fluctuates seasonally. As will be discussed in Section 5.2, we interpret that soil texture controls the persistent spatial pattern seen in each of these figures.

The average water content from each 900 MHz GPR survey shows the effects of seasonal precipitation and irrigation. The May survey occurred at the beginning of the dry season, one week after a light rain, while the August survey was acquired during the dry season, three weeks after the most recent irrigation. The September data were also collected during the dry season,

but only two days after irrigation, and the January data were taken one day after a light rain during the wet season.

The 450 MHz travel time data were also analyzed and converted to water content. The spatial distribution of water content from the 450 MHz data for each campaign is similar, but not identical, to that observed with the 900 MHz data. Also, the average water content obtained from the 450 MHz data for each campaign is slightly higher than that obtained from the 900 MHz data. To investigate the differences between the 900 MHz and 450 MHz data, we subtracted the 900 MHz water content estimates from the 450 MHz estimates for each field grid. Figure 11 shows example plots associated with the 450 MHz data acquired during the September campaign. Figure 11a illustrates the water content field grid estimated using the 450 MHz data, and Figure 11b illustrates the differences in water content estimates between the 450 MHz and 900 MHz data (shown in Figure 10c) for that campaign. Each of the data campaigns revealed a similar trend in the differences. The residuals (the 900 MHz water content estimates subtracted from the 450 MHz estimates) formed similar patterns; the areas that are wet in the original data sets for both frequencies showed the least change in volumetric water content, and the areas that are dry in the original data sets for both frequencies showed the most change. This pattern probably reflects the influence of soil texture on volumetric water content with depth. At this site, the wetter soils are more clay rich, and the clay does not easily release water to near surface evaporation or drainage. The sandier soils usually have lower water contents, and water is more easily lost due to near surface evaporation and drainage. Thus, the 900 MHz data show lower water contents in the drier areas than the 450 MHz data, and the water contents are similar for both frequencies in wetter areas.

Close inspection of the water content distributions in Figures 10 and 11 reveals that adjacent traverses sometimes have significantly different water contents. The contrasts between adjacent traverses are most notable in the 900 MHz data collected in May and September. As the data were collected only along every fifth row (at 6 m intervals between traverses), the sampling increment perpendicular to the rows was much greater than the sampling increment parallel to the rows (0.1 m). Thus, the water content distribution appears smoother in the direction parallel to the rows compared to the direction perpendicular to the rows. Additionally, crop cover (zorrow fescue grass) was planted only in every other row across the field. The crop cover is planted in the fall and begins to go dormant in early summer, and it is not immediately distinguishable from the native vegetation that grows between the vines in all of the rows. However, the crop cover does appear to affect the near-surface water content under certain conditions. Separate analyses of the rows with and without crop cover show that crop cover reduces the water content slightly during the dry season (average reduction of 0.01). The differences in the average water content in rows with and without crop cover were greatest in the 900 MHz data collected during the dry season, while the 450 MHz data were less affected by crop cover for each of the campaigns. These results indicate that the influence of crop cover is more significant in very shallow soils, and probably reflect the root depth of the fescue grass. The influence of crop cover also seems to have a seasonal component, as the water content estimates collected during the dry months have greater differences between rows with and without crop cover than do the estimates collected in January, when the grass is first emerging. In Figures 10 and 11, some of the 'stripey' appearance of adjacent vineyard rows is a manifestation of the change in water content caused by the presence or absence of crop cover.

5.2. Comparison of GPR-estimated water content and soil texture

The correlation of water content and percent sand observed in the DSAs (Section 4.6 and Figure 9) implies that the spatial distribution of water content estimated at one point in time using GPR data is influenced by the soil texture in the near subsurface. A contour plot of the near-surface percent sand at this site is shown in Figure 12. Most of the 40 measurements used to create this plot are from near-surface samples that extend from the ground surface to 20 cm depth. However, some of the measurements were collected from the uppermost 30 cm of the boreholes. (By comparing measurements collected in the 0-20 cm interval with nearby 0-30 cm borehole samples, we observed that the soil texture does not change significantly between the two depth intervals.) Comparison of Figure 12 with Figures 10 and 11 suggests that the spatial pattern of the percent sand measurements is very similar to the GPR-derived water content patterns. Areas of high percent sand correspond to the areas that are consistently dryer on the GPR-obtained water content maps. The zones with low percent sand are consistently wetter. This observation is consistent with the results obtained in the DSAs, as shown in Figure 9. While the observed pattern similarities could potentially be used for estimation of shallow soil textures, the relationship is probably not valid for deeper soils, where the moisture flux is more dependent on time and depth. Additionally, correlations between water content and soil texture are most applicable in areas without appreciable topographic change and where agricultural practices that alter the soil structure or microtopography (such as furrowing) are not performed, as both of these factors could have a much greater impact on water content than does soil texture.

6. Summary

This experiment has shown that GPR groundwave data can be used as a field tool to non-invasively and rapidly estimate shallow water content in a field scale application. Analysis of groundwave travel time data produced water content estimates with a spatial sampling density

much greater than that obtainable using conventional point measurement techniques. The differences between common-offset GPR estimates of water content and gravimetrically derived measurements were generally small, having a volumetric water content RMSE of 0.011 for the 900 MHz data and 0.017 for the 450 MHz data, with the greatest errors occurring in very dry soils. Comparison of 900 MHz and 450 MHz data revealed differences in water content estimates, although the spatial distribution of water content was similar for both frequencies. In general, the 450 MHz data yielded slightly wetter average water contents. Although more controlled experiments are necessary to definitively determine how the depth of influence of the groundwave varies with frequency, the differing average water contents and spatial distributions observed in this experiment suggests that multi-frequency GPR data should be able to estimate the water content at different depths. Estimates of water content from GPR data may also potentially be used to infer soil texture, as seen from the similarity of the GPR water content and soil texture maps. However, this inference will likely only be applicable on sites where the water content is not greatly influenced by topography or agricultural practices.

The results from this experiment can be applied to improve agricultural practices. By estimating the soil water content before starting irrigation, the optimal scheduling and amount of irrigation can be determined. Also, irrigation can be applied non-uniformly across a field as needed. The GPR estimates of water content could also be used to indicate soil texture where the influence of other variables (such as topography) are minimal, so calibrated GPR measurements could be used to identify poor soil conditions and to optimize the planning of vineyard layout (geometry and plant density) and agricultural practices for new vineyards. GPR is a useful tool for these applications because it provides a data density that is unparalleled by any other precision agriculture field tool for water content estimation.

The results presented in this study show that GPR groundwaves can be used as a field tool for estimating volumetric water content. To our knowledge, this analysis is the first time that volumetric water content has been estimated with high resolution over a large-scale heterogeneous field site with measurements collected over both space and time. The detailed water content information collected using this method could be used as input to vadose zone and meteorological modeling, precision agriculture, and water resources management.

Acknowledgements

This study was funded by USDA 2001-35102-09866, NSF EAR-0087802, and WRC project W-929 to Yoram Rubin. We sincerely thank Daniel Bosch and the Robert Mondavi Winery for providing vineyard access and technical information. We also thank Lee Johnson (CSU Monterey Bay and NASA/Ames Research Center) for providing access to the remote sensing imagery. Finally, we wish to thank Andrew Binley, the associate editor who carefully handled this manuscript, and three anonymous reviewers, whose insightful suggestions greatly improved the focus and organization of this manuscript. All computations were carried out at the Center for Computational Seismology (CCS), supported by DOE's office of Basic Energy Sciences, at Lawrence Berkeley National Laboratory.

References

Annan, A.P., Ground Penetrating Radar Workshop Notes, Sensors & Software Inc., PEMD 217, Ontario, Canada, July 2002.

Berktold, A., K.G. Wollny, and H. Alstetter, Subsurface moisture determination with the ground wave of GPR, Proc. Int. Conf. Ground Penetrating Radar 7th, Lawrence, Kansas, USA, Vol. 2, Radar Systems and Remote Sensing Laboratory, Univ. of Kansas, KS, 675-680, 1998.

Carothers, J., Imagery technology meets vineyard management, *Practical Winery and Vineyard*, 54-62, May 2000.

Davis, J.L. and A.P. Annan, Ground penetrating radar for high-resolution mapping of soil and rock stratigraphy, *Geophys. Prosp.*, 37, 531-551, 1989.

Du, S. and P. Rummel, Reconnaissance studies of moisture in the subsurface with GPR, Proc. Int. Conf. Ground Penetrating Radar 5th, Kitchener, Ontario, Canada, Vol. 3, Waterloo Centre for Groundwater Res., Univ. of Waterloo, ON, 1241-1248, 1994.

Greaves, R.J., D.P. Lesmes, J.M. Lee, and M.N. Toksoz, Velocity variations and water content estimated from multi-offset ground penetrating radar, *Geophysics,* 61, 683-695, 1996.

Grote, K., S. Hubbard, and Y. Rubin, GPR monitoring of volumetric water content in soils applied to highway construction and maintenance, *Leading Edge*, 482-485, 2002.

Hagedoorn, J., A process of seismic reflection interpretation, *Geophys. Prosp*., 2, 85-127, 1954.

Herkelrath, W.N., S.P. Hamburg, and F. Murphy, Automatic, real time monitoring of soil moisture in a remote field area with time domain reflectometry, *Water Resour. Res.,* 22(5), 857-864, 1991.

Hubbard, S., J.E. Peterson, E.L. Majer, P.T. Zawislanki, K.H. Williams, J. Roberts, and F.

Wobber, Estimation of permeable pathways and water content using tomographic radar data, *Leading Edge*, 1623-1628, 1997.

Huisman, J.A., C. Sperl, W. Bouten, and J.M. Berstraten, Soil water content measurements at different scales: accuracy of time domain reflectometry and ground penetrating radar, *J. Hydrol.*, 245, 48-58, 2001.

Huisman, J.A. and W. Bouten, Mapping surface soil water content with the ground wave of ground-penetrating radar, Proc. Int. Conf. Ground Penetrating Radar 9th, Santa Barbara, California, USA, Vol. 1, Bechtel Nevada/Special Technologies Laboratory, Univ. of California, Santa Barbara, CA, 162-169, 2002.

Jackson, T.J., J. Schmugge, and E.T. Engman, Remote sensing applications to hydrology: soil moisture, *Hydrological Sciences*, 41(4), 517-530, 1996.

Johnson, L., R. Nemani, L. Pierce, M. Bobo, and D. Bosch, Toward the improved use of remote sensing and process modeling in California's premium wine industry, Proc. IEEE International Geoscience and Remote Sensing Symposium, Vol. 1, 363-365, 2000.

Lambert, G., J. Kashiwagi, B. Hansen, P. Gale, and A. Endo, Soil Survey of Napa County, California, USDA Soil Survey, U.S. Gov. Printing Office, Washington, D.C., 1978.

Lesmes, D., R.J. Herbstzuber, and D. Wertz, Terrain permittivity mapping: GPR measurements of near-surface soil moisture, Proc. Symp. Applications of Geophysics to Engineering and Environmental Problems, Environmental and Engineering Geophysical Society, 575-582, 1999.

Mancini, M., R. Hoeben, and P. A. Troch, Multifrequency radar observations of bare surface soil moisture content: A laboratory experiment, *Water Resour. Res.,* 35(6), 1827-1838, 1999.

Mauser, W., M. Rombach, H. Bach, A. Demircan, and J. Kellndorfer, Determination of spatial

and temporal soil-moisture development using multitemporal ERS-1 data, Proc. SPIE Multispectral and Microwave Sensing of Forestry, Hydrology, and Natural Resources, Vol. 2314, 502-515, 1994.

Olhoeft, G.R. and D.E. Capron, Petrophysical Causes of Electromagnetic Dispersion, Proc. Int. Conf. Ground Penetrating Radar 5th, Kitchener, Ontario, Canada, Vol. 1, Waterloo Centre for Groundwater Res., Univ. of Waterloo, ON. 145-152, 1994.

Penn, C., Grape growers gravitating toward space age technologies, *Wine Business Monthly*, 53-56, Feb. 1999.

Prichard, T., Soil moisture measurement technology, Wine Grape Irrigation Short Course, University of California at Davis Extension, Davis, California, 1999.

Sakaki, T., K. Sugihara, T. Adachi, K. Nishida, and W. Lin, Application of time domain reflectometry to determination of volumetric water content in rock, *Water Resour. Res.,* 34(10), 2623-2631, 1998.

Saxton, K.E., W.J. Rawls, J.S. Romberger, and R.I. Papendick, Estimating generalized soil-water characteristics from texture, *Soil Sci. Soc. Amer. J.*, 50(4), 1031-1036, 1986.

Topp, G.C., J.L. Davis, and A.P. Annan, Electromagnetic determination of soil water content: measurements in coaxial transmission lines, *Water Resour. Res.,* 16(3), 574-582, 1980.

Van Overmeeren, R., S. Sariowan, and J. Gehrels, Ground penetrating radar for determining volumetric soil water content: results of comparative measurements at two test sites, *J. Hydrol.* 197, 316-338, 1997.

Western, A.W., G. Blöschl, and R. B. Grayson, Geostatistical characterization of soil moisture patterns in the Tarrawara catchment, *J. Hydrol*., 205, 20-37, 1998.

White, I. and S.J. Zegelin, Electric and dielectric methods for monitoring soil-water content, In:

Handbook of vadose zone characterization and monitoring, Chapter 22, L.G. Wilson, L.G. Everett, and S. Cullen (Eds.), Lewis Publ., Ann Arbor, MI, 1995.

Yilmaz, O., *Seismic Data Processing*, Society of Exploration Geophysicists, Tulsa, OK, 1999.

Figure Captions

Figure 1 Site map showing the field grid lines and the positions of the dense sampling areas (DSAs) superimposed on normalized difference vegetation index (NDVI) imagery acquired during July 2000. The x-axis on this map is the number of the vineyard row, and the y-axis is the vine number.

Figure 2 900 MHz GPR data collected in Row 115 in January. Figure 2a) CMP survey at vine 60. The x-axis is the antenna separation, and the y-axis is the travel time of the GPR signal. Positive amplitudes are shown as peaks (black) and negative amplitudes are shown as troughs (white). Figure 2b) Common-offset traverse along vines 48-65. The x-axis is distance along the traverse, and the y-axis is the travel time of the GPR signal.

Figure 3 450 MHz GPR data collected in Row 35 in January. Figure 3a) CMP survey at vine 50. Figure 3b) Common-offset traverse along vines 41-58.

Figure 4 900 MHz common-offset traverse collected after performing an infiltration experiment in dry soil. The airwave and groundwave are distinct in the wet soil in the middle of the traverse, but are partially superimposed in the surrounding dry soil. The main trough and peak normally picked for the airwave and groundwave are shown, as are the adjusted picks and the correction factors that can be used to calculate a more accurate travel time difference.

Figure 5 Comparison of electromagnetic velocity estimated from CMP and common-offset surveys for 900 MHz and 450 MHz data. The correlation between velocities from both surveying methods indicates that the common-offset data interpretation procedure is reasonable.

Figure 6 A site-specific petrophysical relationship developed using measurements from TDR, gravimetric water content, and soil texture collected in the DSAs.

Figure 7 Validation of the groundwave picking procedure and site-specific petrophysical relationship in CMP and common-offset data. Figure 7a) Comparison of volumetric water content (VWC) estimates derived from 900 MHz and 450 MHz CMP data collected at the DSAs with coincident volumetric water content measurements obtained gravimetrically. Figure 7b) Comparison of volumetric water content estimates derived from common-offset 900 MHz and 450 MHz data collected at the DSAs with coincident volumetric water content measurements obtained gravimetrically.

Figure 8 Comparison of dielectric constant (κ) estimates from TDR and common-offset GPR collected in the DSAs.

Figure 9 Comparison of shallow soil texture, quantified as percent sand, with volumetric water content derived from gravimetric sampling during the detailed studies.

Figure 10 Comparison of the volumetric water content distribution estimated using 900 MHz common-offset travel time data over the entire field at four times throughout a nine month period: 10a) Data from May 2001, 10b) Data from August, 2001, 10c) Data from September 2001, 10d) Data from January 2002. The spatial pattern of water content at this site is similar over time, although the absolute water content values fluctuate seasonally and with irrigation.

Figure 11 Comparison of the water content estimates from 900 MHz and 450 MHz data. Figure 11a) Water content estimates from 450 MHz common-offset travel time data collected over the entire field in September 2001. Figure 11b) Differences between 900 MHz and 450 MHz common-offset estimates of volumetric water content collected over the entire field in September 2001, which indicates that the greatest differences in water content between the two frequencies occur in drier soils having higher sand content.

Figure 12 Contour map of the percent sand in shallow soil measurements collected during the detailed studies and during borehole excavation. The locations of the data points used to generate this image are shown in Figure 1. The spatial pattern produced by soil texture is similar to the water content distribution spatial patterns shown in Figures 10 and 11.

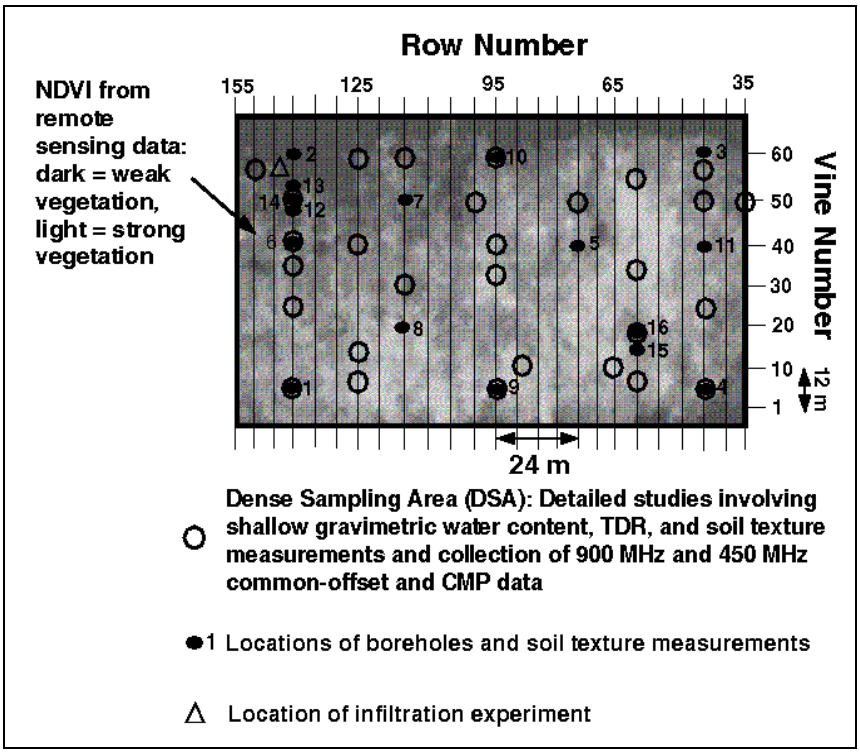
Row Number
155
125
95
65
35
NDVI from remote sensing data: dark = weak vegetation, light = strong vegetation
Vine Number
60
50
40
30
20
10
1
12 m
24 m
Dense Sampling Area (DSA): Detailed studies involving shallow gravimetric water content, TDR, and soil texture measurements and collection of 900 MHz and 450 MHz common-offset and CMP data
1 Locations of boreholes and soil texture measurements
Location of infiltration experiment

Figure 1

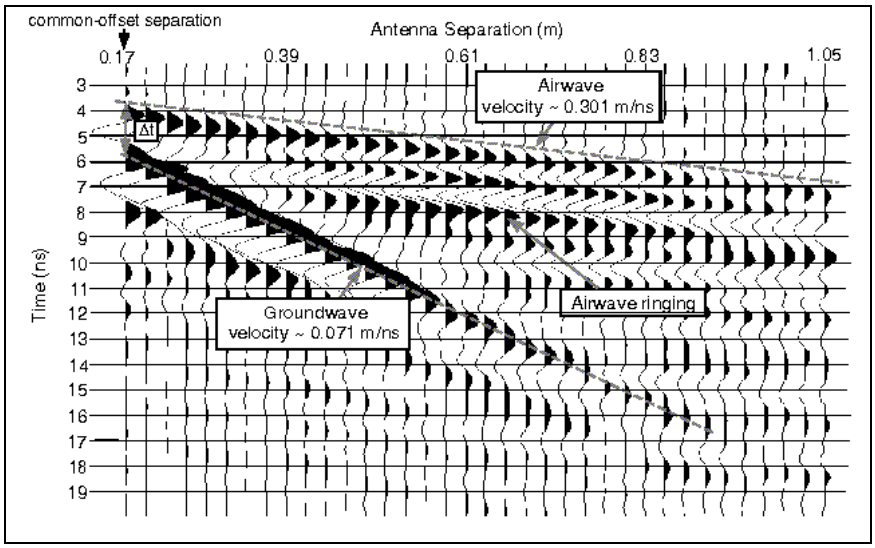

Figure 2a

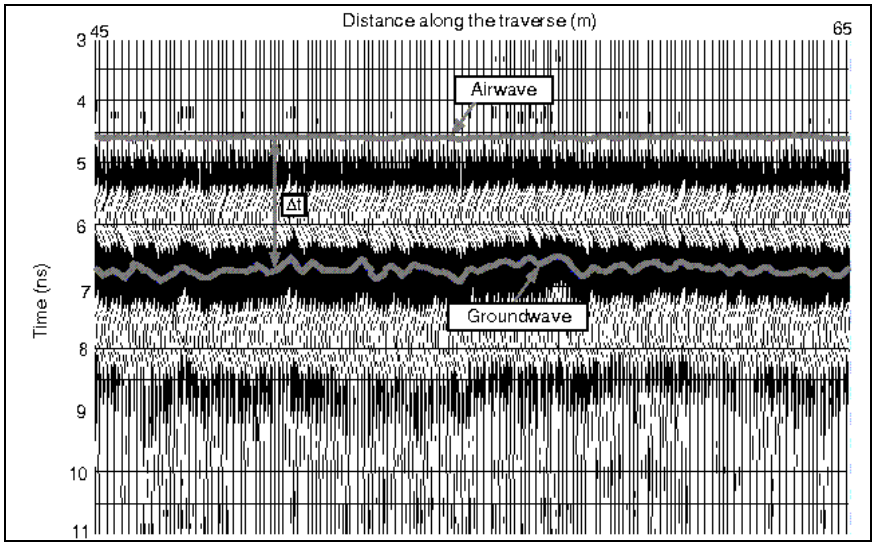

Figure 2b

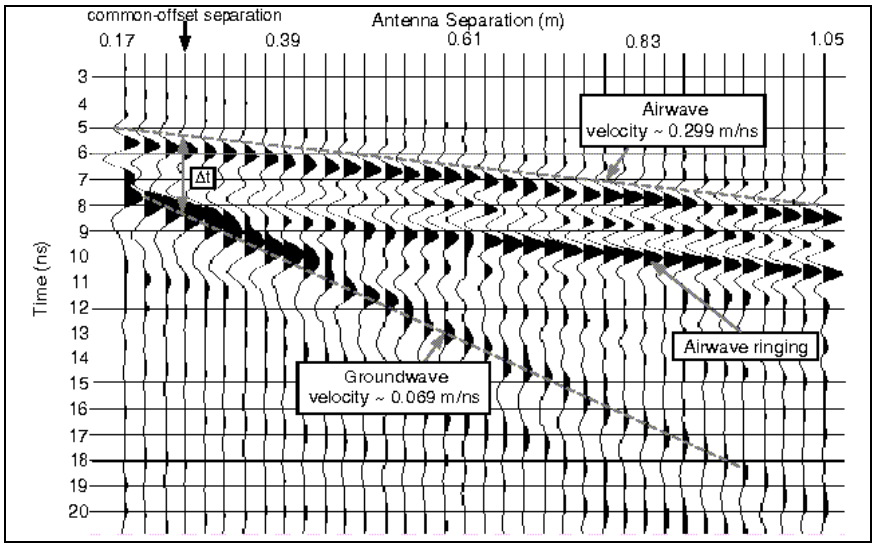

Figure 3a

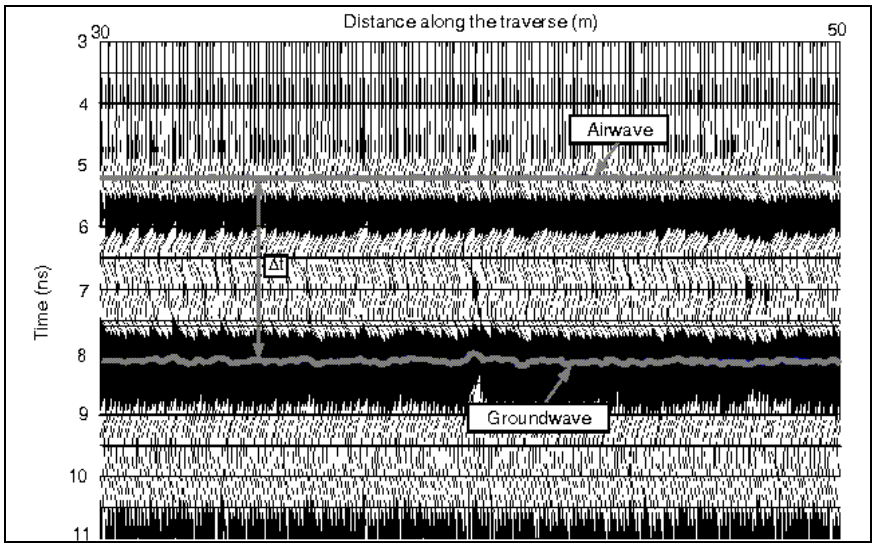

Figure 3b

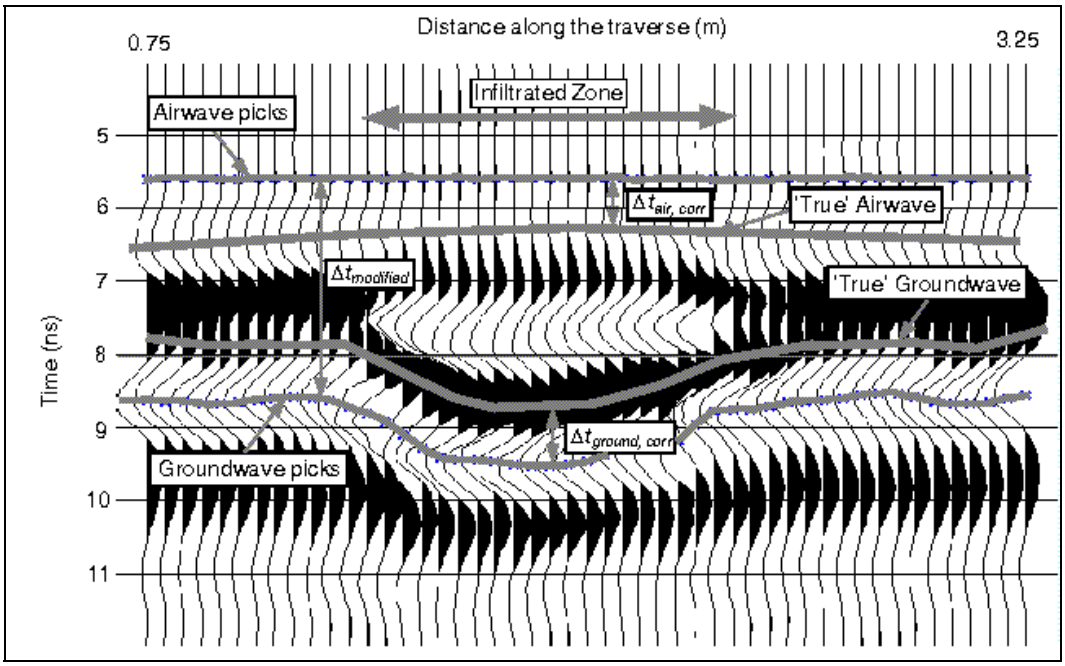
Distance along the traverse (m)
0.75
3.25
Airwave picks
Infiltrated Zone
$\Delta t_{air,\ corr}$
'True' Airwave
$\Delta t_{modified}$
'True' Groundwave
$\Delta t_{ground,\ corr}$
Groundwave picks
Time (ns)
5
6
7
8
9
10
11

Figure 4

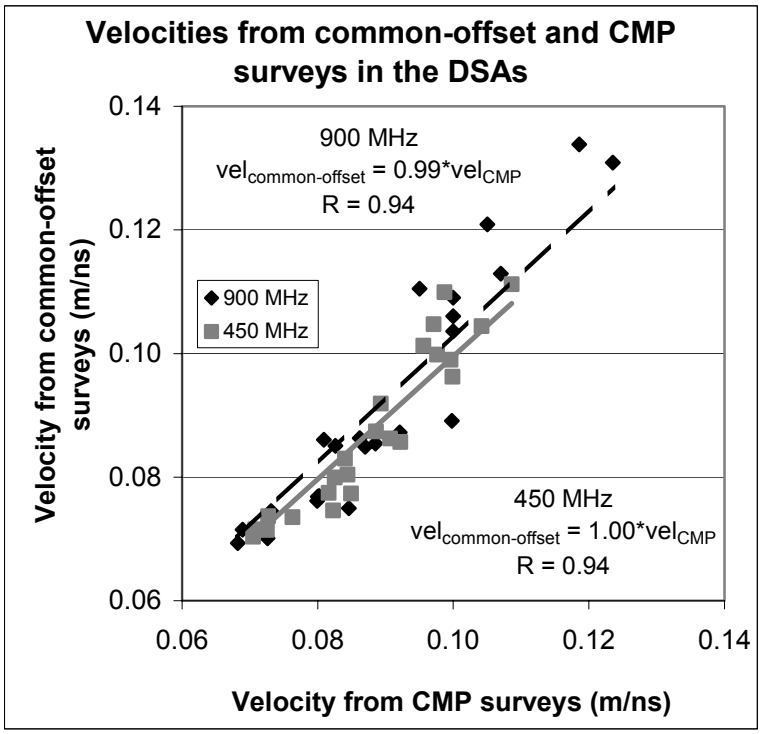

Figure 5

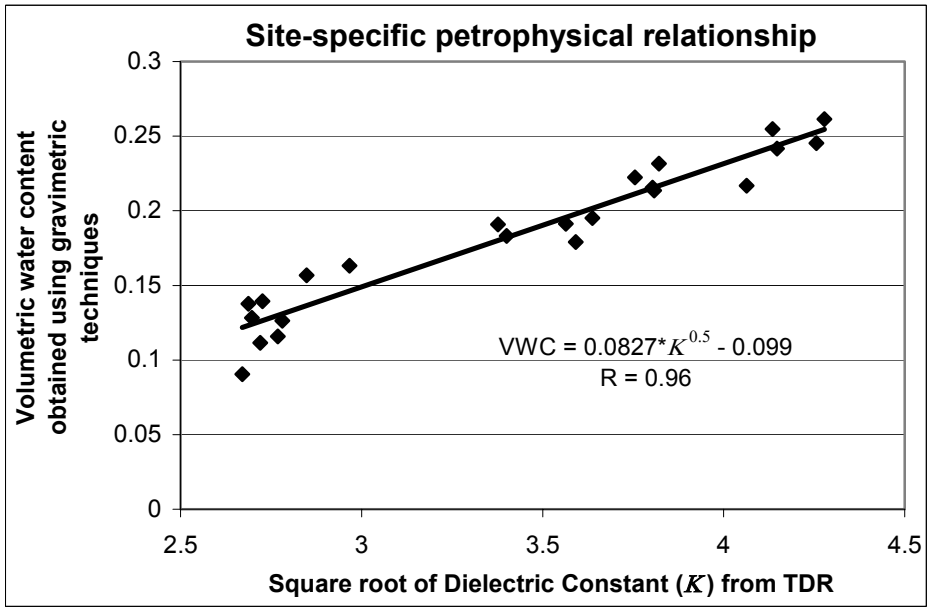

Figure 6

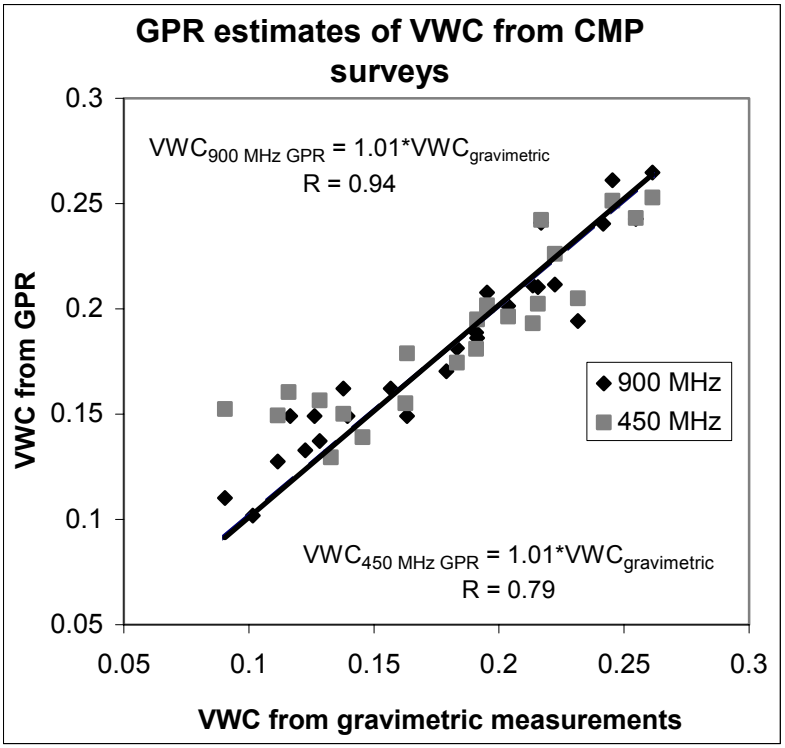

Figure 7a

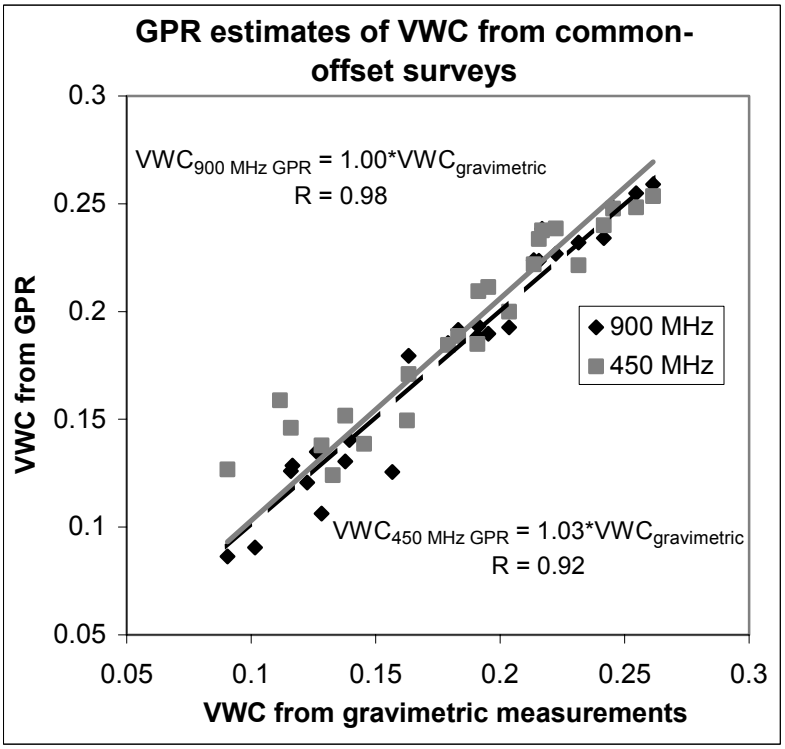

Figure 7b

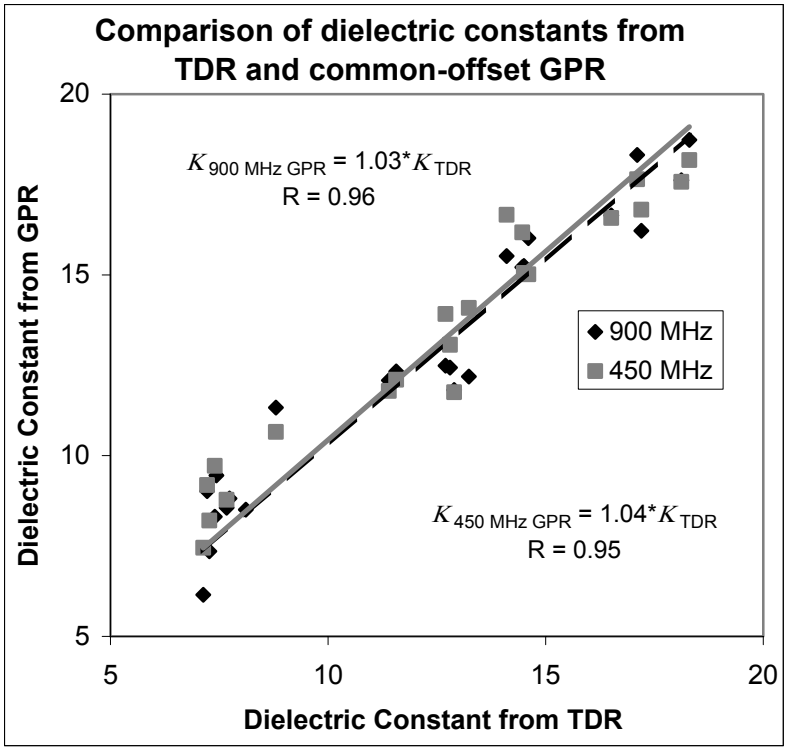

Figure 8

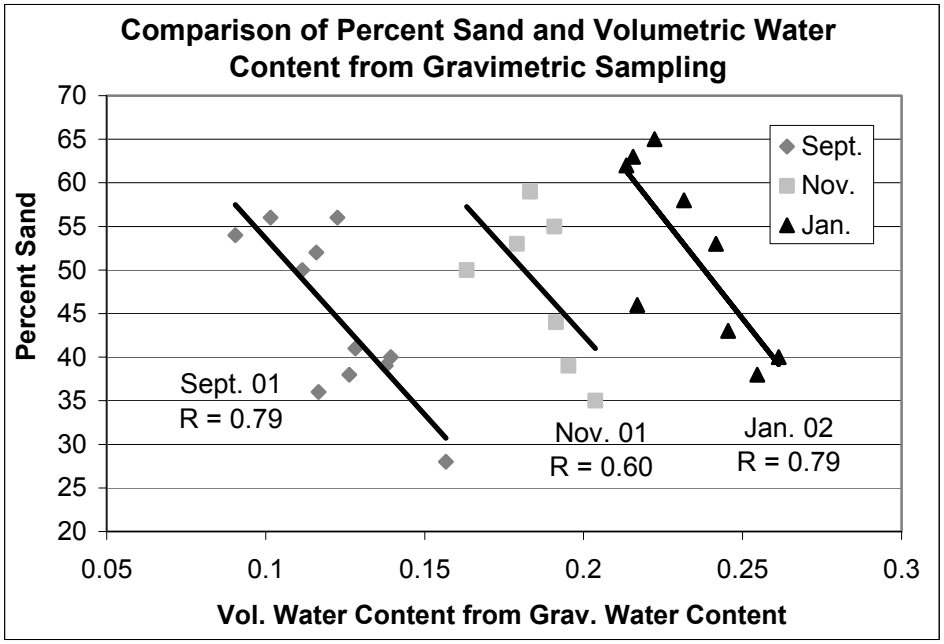

Figure 9

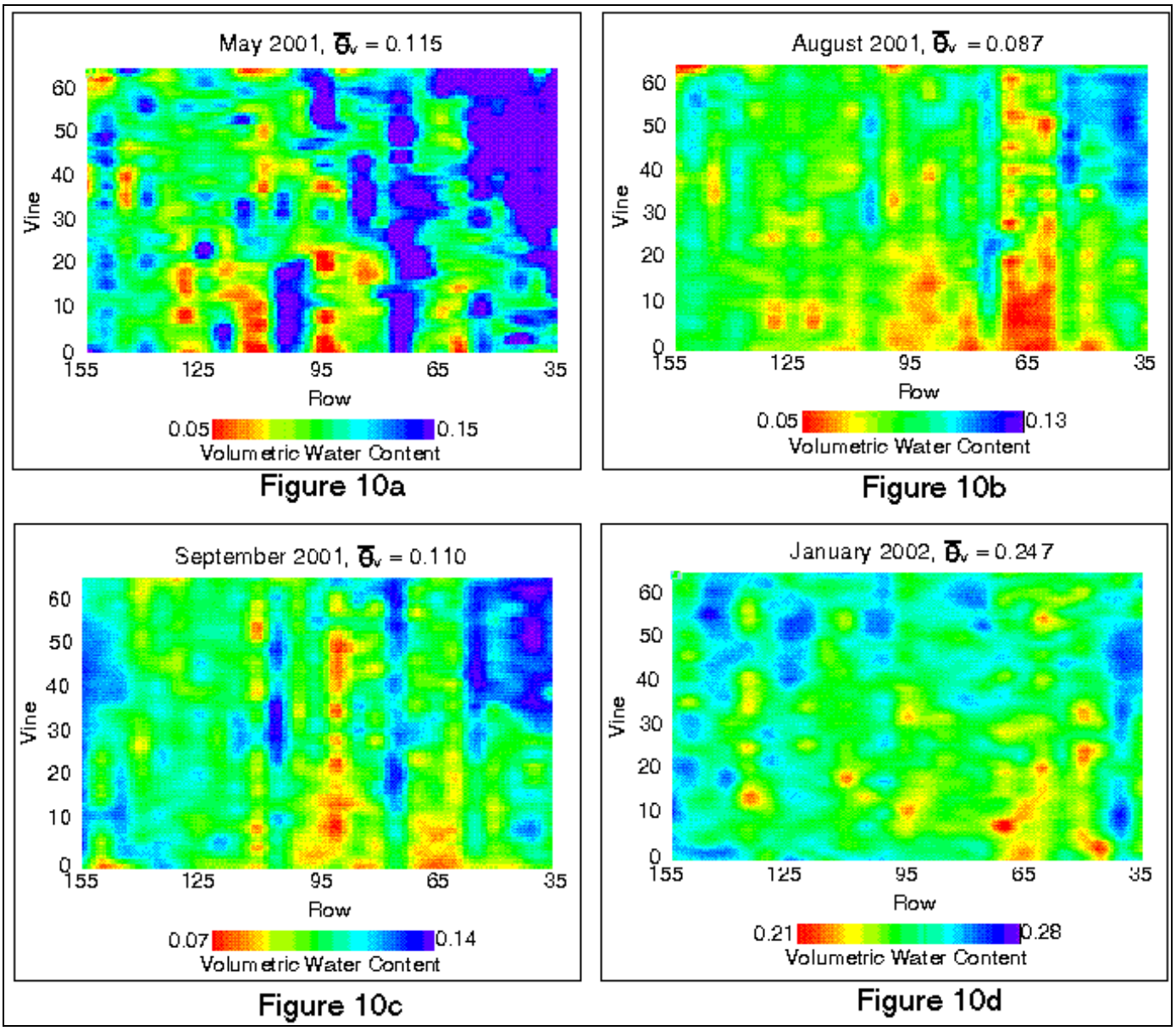
May 2001, $\overline{\theta}_v$ = 0.115
Vine
Row
0.05
0.15
Volumetric Water Content
Figure 10a
August 2001, $\overline{\theta}_v$ = 0.087
Vine
Row
0.05
0.13
Volumetric Water Content
Figure 10b
September 2001, $\overline{\theta}_v$ = 0.110
Vine
Row
0.07
0.14
Volumetric Water Content
Figure 10c
January 2002, $\overline{\theta}_v$ = 0.247
Vine
Row
0.21
0.28
Volumetric Water Content
Figure 10d

Figure 10

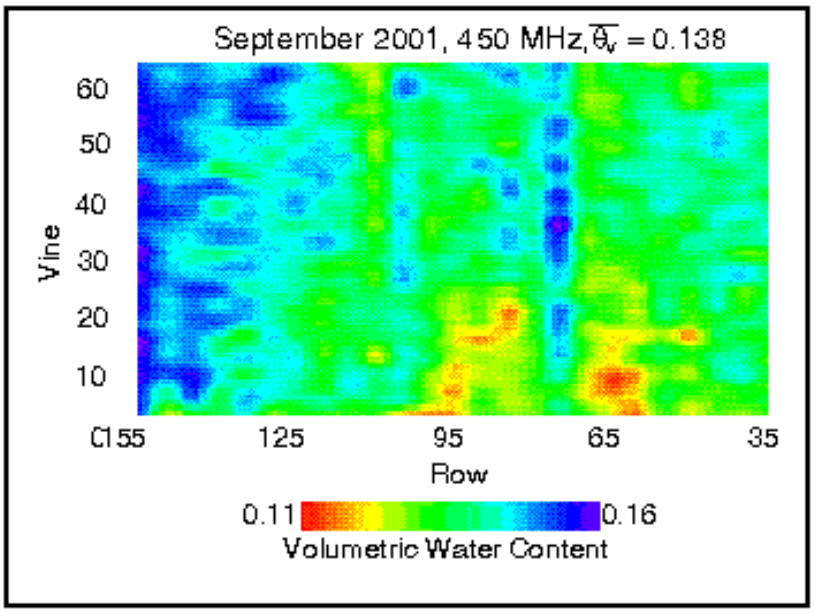

Figure 11a

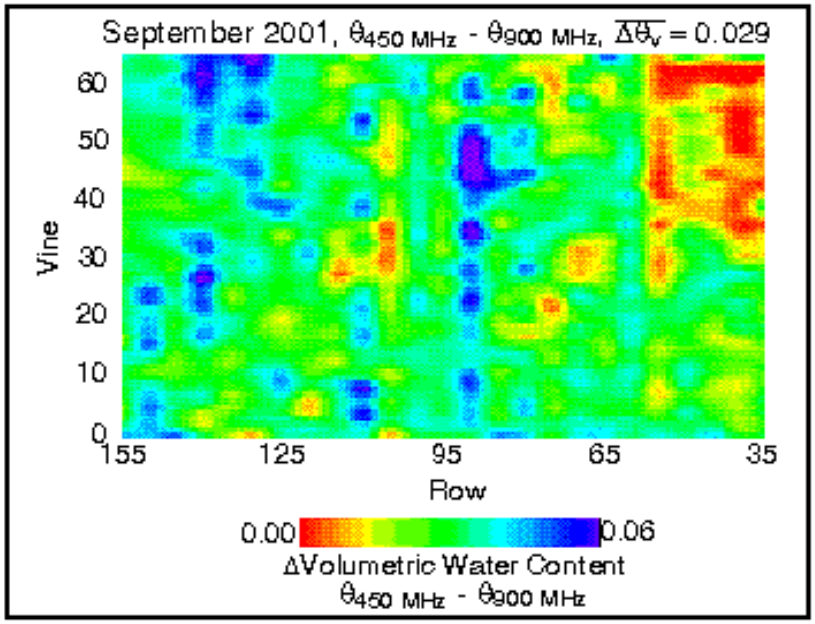

Figure 11b

Figure 11

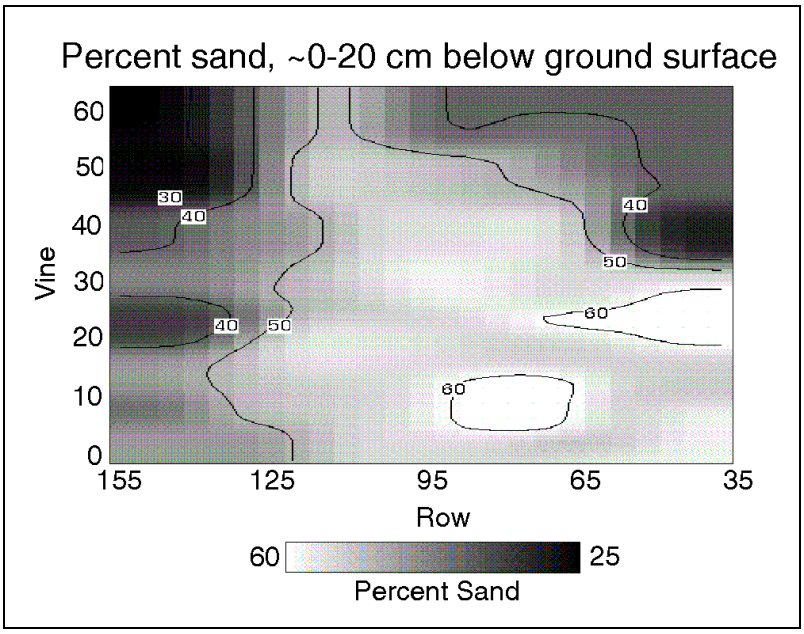
Percent sand, ~0-20 cm below ground surface
Vine
60
50
40
30
20
10
0
30
40
40
50
40
50
60
60
155
125
95
65
35
Row
60
25
Percent Sand

Figure 12